Dynamic Behavior of Threshold Voltage and I_D–V_{DS} Kink in AlGaN/GaN HEMTs Due to Poole–Frenkel Effect

Zhan Gao, *Member, IEEE*, Carlo De Santi, *Member, IEEE*, Fabiana Rampazzo,
Marco Saro, *Graduate Student Member, IEEE*, Mirko Fornasier, *Member, IEEE*,
Gaudenzio Meneghesso, *Fellow, IEEE*, Matteo Meneghini, *Senior Member, IEEE*,
Alessandro Chini, Giovanni Verzellesi, *Senior Member, IEEE*,
and Enrico Zanoni, *Life Fellow, IEEE*

***Abstract*—The kink effect in field-effect transistors (FETs) consists in a sudden increase in drain current, I_D, during a drain voltage sweep and leading to a higher I_D saturation value. We report new experimental data concerning the dynamic behavior of the "kink" in AlGaN/GaN HEMTs and correlate them with deep levels. The results demonstrate the role of the Poole–Frenkel effect in determining the occurrence of the kink and identify the experimental conditions that make it observable.**

***Index Terms*—Current collapse, deep levels, GaN HEMT, GaN reliability, kink effect.**

I. INTRODUCTION

DRAIN current, I_D, versus drain voltage, V_{DS}, characteristics of field-effect transistors (FETs) can be affected by an instability called "kink effect," which consists in a sudden increase in I_D during a V_{DS} sweep, taking place over a narrow V_{DS} range and leading to a higher I_D saturation value [1]. The kink effect has been observed in silicon-on-insulator and silicon-on-sapphire MOSFETs, where it has been attributed to accumulation of positive charge in the floating Si buffer due to holes generated by impact ionization [2], [3], [4]. GaAs FETs can be affected by kink due to trapping/detrapping effects in the semi-insulating substrate or at the device surface [5], [6].

More recently, the kink effect has been reported both in Ga-polar [1], [7], [8], [9], [10], [11], [12], [13], [14], [15], [16], [17], [18], [19] and in N-polar GaN HEMTs [20] and attributed to surface-related traps [8], [21], [22], [23], impact ionization [9], [20], [24], [25], strongly field-dependent detrapping processes from deep acceptor states in the vicinity of the gate [6], [11], donor-like traps in the GaN buffer layer [12], [26], slow donor-like traps located under or near the gate [7], [19], and charging effects related to generation and transport of holes in a floating, C-doped p-type buffer [13], [15], [16], [17], [18].

The kink effect can be associated with transconductance decrease and output conductance increase [14], [28], [29] and is therefore a relevant degradation mechanism for GaN HEMTs, which currently represent the most promising devices for RF power amplifier applications [29], [30]. Recently, Grupen [1] has investigated kink effects in GaN HEMTs by means of simulations based on the Fermi kinetics transport and hot electron simulation method, including field-enhanced tunneling ionization of deep traps. Simulations in [1] were compared with experimental data reported in [12]; it was shown that the highly nonlinear field dependence of the electron tunneling probability into and out of traps located in the AlGaN barrier, along with hot electron effects, can explain the shape and bias dependence of the kink effect.

In this article, we report new experimental data concerning the dynamic behavior of the kink effect in GaN HEMTs, an aspect that has been neglected in the literature up to now. Results confirm the model proposed in [1] and provide new insights concerning the experimental characterization of kink effects. Devices under test, experimental setup, and experimental procedures are introduced in Section II; experimental results concerning direct current (dc) characteristics and dynamic threshold voltage, and V_{TH} transient results are discussed in Section III. Finally, the results are reviewed and discussed in Section IV.

Manuscript received 23 August 2023; revised 27 September 2023; accepted 19 October 2023. Date of publication 31 October 2023; date of current version 28 November 2023. This work was supported in part by the Italian Ministry of Research Progetti di Rilevante Interesse Nazionale (PRIN) Project "Empowering GaN-on-SiC and GaN-on-Si Technologies for the Next Challenging Millimeter-Wave Applications"; in part by the U.S. Office of Naval Research (supervisor Paul Maki) under Award N000142012177; and in part by the European Commission Horizon 2020 European Centre for Science, Ethics and Law (ECSEL) Initiative Project 5G_GaN2. The review of this article was arranged by Editor M. Hua. *(Corresponding author: Zhan Gao.)*

Zhan Gao, Carlo De Santi, Fabiana Rampazzo, Marco Saro, Mirko Fornasier, Gaudenzio Meneghesso, and Enrico Zanoni are with the Department of Information Engineering, University of Padova, 35131 Padua, Italy (e-mail: zhan.gao@unipd.it).

Matteo Meneghini is with the Department of Information Engineering and the Department of Physics and Astronomy, University of Padova, 35131 Padua, Italy.

Alessandro Chini is with the Department of Engineering "Enzo Ferrari," University of Modena and Reggio Emilia, 41126 Modena, Italy.

Giovanni Verzellesi is with the Department of Sciences and Methods for Engineering, University of Modena and Reggio Emilia, 41126 Modena, Italy.

Color versions of one or more figures in this article are available at https://doi.org/10.1109/TED.2023.3326781.

Digital Object Identifier 10.1109/TED.2023.3326781

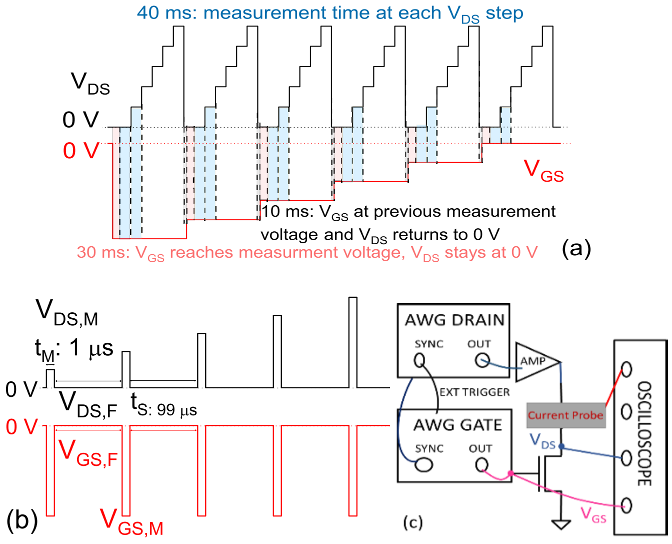

Fig. 1. Schematic of the measurment processes during (a) DC characterization: first, the V_{GS} value is set, and after 30 ms (pink), the staircase V_{DS} ramp starts; each step having a minimum duration of 40 ms (blue); at the end of the last step, when V_{DS} reaches V_{DSmax}, the drain voltage is turned off, after approximately 10 ms (black), the new V_{GS} is applied (b) DP characterizations and (c) setup of the DP system.

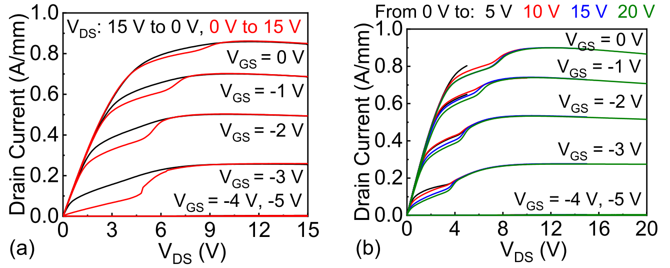

Fig. 2. (a) I_D–V_{DS} characteristics with forward (V_{DS} from 0 to 15 V) and reverse (15 to 0 V) sweeps, 0.1-V steps. (b) Forward I_D–V_{DS} with V_{DS} swept up to 5, 10, 15, and 20 V. Sweep speed 40 ms/V. V_{GS} is swept from −5 V up to 0 V.

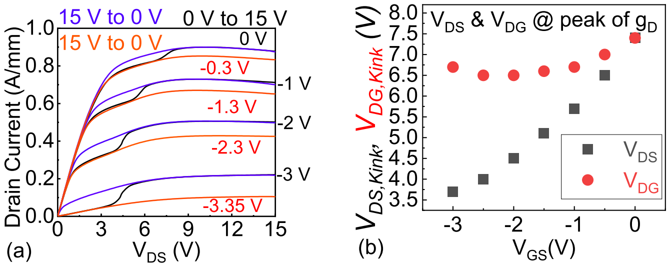

Fig. 3. (a) I_{DS}–V_{DS} sweeps with different V_{GS}'s during forward sweep (0 to 15 V) and reverse sweep (15 to 0 V) at different V_{GS}'s. (b) Position of the kink ($V_{DS,Kink}$ $V_{DG,Kink}$) as a function of V_{GS} and V_{DG}.

II. EXPERIMENTAL DETAILS: DEVICES, QUASI-STATIC, AND PULSED I_D–V_{DS} CHARACTERISTICS

The devices analyzed in this article were fabricated on AlGaN/GaN heterostructures grown on SiC substrate, by using a 0.25-μm standard industry process. The GaN buffer was doped with carbon (C), in order to increase the charge confinement and reduce short-channel effects. MOCVD epitaxial growth of AlGaN/GaN ended with the growth of an in situ SiN passivation layer, which was subsequently selectively removed by an Ar plasma treatment before depositing the Pt/Ni/Au gate metallization. The devices under test have a total gate width of 2 × 50 μm and a gate-to-drain distance (L_{GD}) of 4 μm. A maximum current of 0.85 ± 0.03 A/mm, a maximum transconductance of 330 ± 20 ms/mm, and an OFF-state gate leakage current of 22 ± 6.1 μA/mm are achieved. A Keysight E5263A semiconductor device parameter analyzer was adopted to measure the dc device I_D–V_{DS} output characteristics, using step gate voltage (V_{GS}) and staircase drain voltage (V_{DS}) sweep.

During the dc measurement, a V_{GS} value is set; after 30 ms, the staircase V_{DS} ramp starts, each step having a minimum duration of 40 ms [one power line cycle (PLC)]. At the end of the last step, with V_{DS} at its maximum value V_{DSmax}, the drain voltage is turned off ($t_{fall} < 0.5$ ms), there is a waiting time of approximately 10 ms, and then, the new value of V_{GS} is applied, as shown in Fig. 1(a).

As an alternative method to measure the I_D–V_{DS} characteristics, a "double-pulse" (DP) system [31] was used [Fig. 1(b)], where V_{DS} and V_{GS} can be pulsed in order to measure the I–V device characteristics starting from a "stress" quiescent bias point, usually with a very low "measure" to "stress" duty cycle, keeping the measurement duration short in order to avoid self-heating and trapping/detrapping effects during measurement. A 1-/99-μs duty cycle was adopted in our case. The DP system is a custom system; based on arbitrary waveform generators (AWGs) and amplifiers (AMP), the drain current is recorded using a current probe, as shown in Fig. 1(c).

Hysteresis in I_D–V_{DS} characteristics is observed when V_{DS} is swept toward higher values and back [Fig. 2(a)]: when the characteristics are measured starting from the maximum drain voltage (V_{DSmax}) and decreasing V_{DS}, the kink disappears. Considering the kink magnitude as the current difference before and after the sharp rise, the kink magnitude increases at increasing V_{DSmax} applied during measurements [Fig. 2(b)].

During the forward and reverse V_{DS} sweep, ON-resistance (R_{ON}) showed no difference; by comparing various forward and reverse sweeps at different V_{GS}, it is evident that the kink is caused by a ≈300-mV V_{GS} difference, equivalent to a positive shift of threshold voltage V_{TH}, as shown in Fig. 3(a). The peak of the output conductance, g_D, corresponds to the position of the kink and occurs at an almost constant value of $V_{DG} \cong 6.5$ V, see Fig. 3(b).

When the output characteristics are measured using the DP system, with a measurement time $t_M = 1$ μs after a 99-μs quiescent phase at $V_{GS,S} = V_{DS,S} = 0$ V, the kink disappears. Pulsed curves also show reduced self-heating (smaller decrease of I_{DS} at high V_{DS}) and slightly lower R_{ON} in a linear region, see Fig. 4. DC and DP measurements confirm that the kink in our devices has the same features described in the previous papers.

III. DRAIN CURRENT AND THRESHOLD VOLTAGE TRANSIENTS

The analysis of drain current and threshold voltage transients provides a deeper insight into the origin of kink

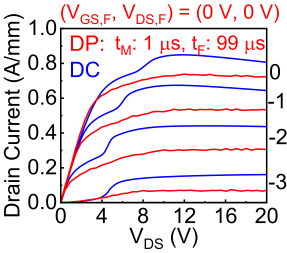

Fig. 4. Comparison of dc output I_D–V_{DS} characteristics with those measured by the DP system with a quiescent bias $V_{GS} = V_{DS} = 0$ V; measurement time $t_M = 1$ μs and quiescent bias time $t_F = 99$ μs.

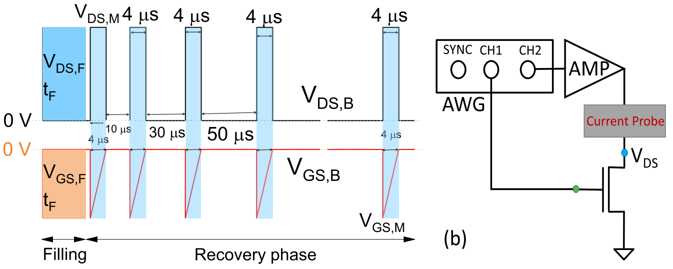

Fig. 5. (a) Bias sequence applied to the gate and drain contact. (b) Simplified schematic diagram of the V_{TH} transient setup used in the work.

effect in the tested devices. The stress/recovery experiment consists in applying a constant ($V_{GS,F}$, $V_{DS,F}$) stress for a fixed duration of time ("filling" phase, up to 100 s typically), then observing the recovery of the device biased at $V_{GS,B}$ and $V_{DS,B}$ ("recovery" phase) for other 100 s. During both the stress and the recovery phases, a set of dynamic fast I_D–V_{GS} measurements at $V_{DS,M}$, with $V_{GS,M}$ from -4.5 to 0 V were carried out with a 4-μs sweep time, at logarithmically spaced time intervals, in order to monitor the current and V_{TH} variation over time, as shown in Fig. 5.

The emission time constant of the involved deep levels could be derived by fitting the current transient curves with stretched multiexponential functions as follows:

$$I_{DS}(t) = I_{DS,\text{final}} + A_0 \exp\left(-\left(\frac{t}{\tau_0}\right)^{\beta_0}\right) + A_1 \exp\left(-\left(\frac{t}{\tau_1}\right)^{\beta_1}\right) \quad (1)$$

where the fitting parameters A_0 and A_1 are amplitudes, τ_0 and τ_1 are the time constant, and β_0 and β_1 are the stretching factors.

Then, the measurements were repeated at different temperatures, from which the Arrhenius plots were extrapolated.

Fig. 6 shows drain current transients at various temperatures; filling was carried out in pinchoff condition (−6, 25 V); a (0, 0 V) bias was applied during recovery. During filling, a significant decrease of I_D occurred within the first 10 μs, followed by a slower decrease. By fitting the transient using the two-stretched exponential function [black dashed lines in Fig. 6(b)], two trapping signatures were extracted during unbiased recovery measurement: the first one (E2) corresponds to the 10 μs–1 ms region observed during recovery and has an activation energy (E_A) equal to 0.8 eV and the second one (E1) is extremely slow and its activation energy is 0.5 eV [Fig. 6(c)].

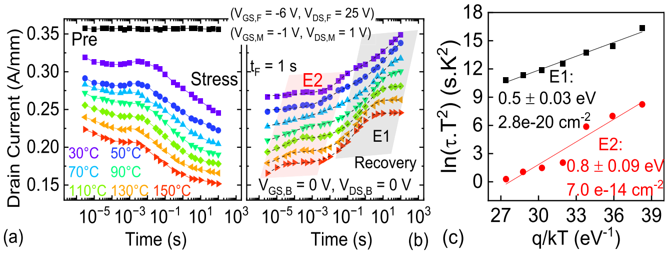

Fig. 6. Repeated measurements at $V_{GS,M} = -1$ V and $V_{DS,M} = 1$ V without bias during recovery ($V_{GS,B} = V_{DS,B} = 0$ V). (a) During stress in pinchoff at $V_{GS,F} = -6$ V and $V_{DS,F} = 25$ V and (b) recovery after 1-s stress at ($V_{GS,F} = -6$ V and $V_{DS,F} = 25$ V), at baseplate temperature from 30 °C to 110 °C; color dot curves: experimental data and black dashed line: fit curves. (c) Arrhenius plots of E1 and E2 during the recovery phase.

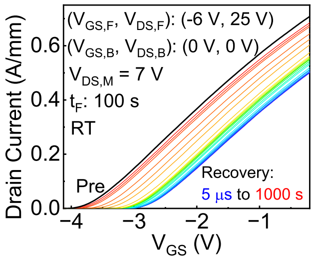

Fig. 7. I_D–V_G curves in linear scale at $V_{DS,M} = 7$ V, $V_{GS,M}$ from −4.5 to 0 V, during the recovery phase, without bias during recovery ($V_{DS,B} = V_{GS,B} = 0$ V), after 100 s stress at $V_{GS,F} = -6$ V and $V_{DS,F} = 25$ V at RT.

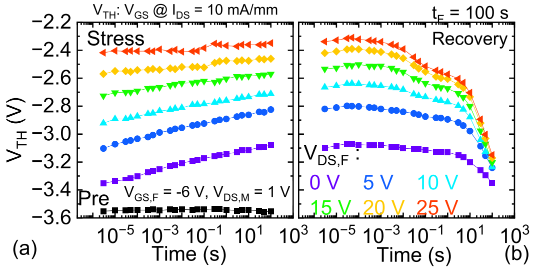

Fig. 8. Dynamic V_{TH} transient with different filling voltage $V_{DS,F}$ in pinchoff at $V_{GS,F} = -6$ V. (a) Filling transient. (b) Recovery at $V_{DS,B} = V_{GS,B} = 0$ V at RT. V_{TH} was extracted as V_{GS} at $I_{DS} = 10$ mA/mm.

The I_D–V_G curves during the recovery phase at RT showed that it takes more than 10^3 s to achieve a complete recovery of the drain current and V_{TH}, as shown in Fig. 7. Due to the fact that the accuracy of the current probe is 1 mA, V_{TH} was extracted as V_{GS} when I_{DS} is 1 mA from the experimental I_D–V_G curves.

Fig. 8 shows the effect of $V_{DS,F}$ during the filling phase at OFF-sate, with $V_{GS,F}$ that is kept at −6 V, and $V_{DS,F}$ increases from 0 to 25 V: the $|V_{TH}|$ value decreases at increasing $V_{DS,F}$, which is consistent with the increase of kink amplitude with $V_{DS,max}$ (Fig. 2).

When a nonzero bias is applied during the recovery phase, significant changes in the transient kinetics occur, see Fig. 9. The E2 transition (corresponding to 0.8-eV activation energy) is not affected by gate voltage; on the contrary, the emission

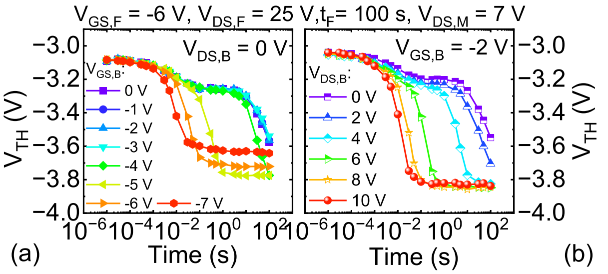

Fig. 9. Dynamic V_{TH} recovery transient of the device under test after a 100-s filling at $V_{GS,F} = -6$ V and $V_{DS,F} = 25$ V with different (a) gate voltage $V_{GS,B}$ values applied during the recovery at $V_{DS,B} = 0$ V and (b) drain voltage $V_{DS,B}$ values applied during the recovery at $V_{GS,B} = -2$ V.

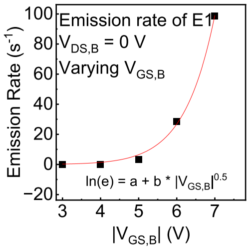

Fig. 10. Emission rate (e) of E1 as a function of the applied $V_{GS,B}$.

time constant of the E1 transition is reduced from 10^2 to 10^{-2} s when V_{GS} goes from 0 to −7 V with $V_{DS,B} = 0$ V.

Notice that $V_{GS} < -5$ V (in pinchoff) induces electron trapping during the recovery phase, leading to positive shift of threshold voltage, see Fig. 9(a); on the contrary, when $V_{GS} = -2$ V (ON-state), a drain voltage value as high as $V_{DS,B} = 10$ V is needed to move the E1 transition to 10^{-2} s; no extra trapping occurs after 100 s at $V_{GS,B} = -2$ V, $V_{DS,B} = 10$ V, and V_{TH} recovers to the value measured without stress, see Fig. 9(b).

The functional dependence on the electric field of the emission rate $e = (\tau)^{-1}$ of E1 (the trap responsible for the kink effect) is determined by fitting the emission rate using a power law function ($\ln(e) = a + b * V^p$). The fitting parameter p is 0.5 (Fig. 10), proving that e increases exponentially with the square root of the bias voltage, i.e., of the electric field, in agreement with the generally accepted model for Poole–Frenkel effect [32].

By fitting e as a function of $\sqrt{V}_{GS,B}$ using

$$e = e(0)\exp\left(\alpha\sqrt{V}_{GS,B}\right)$$

the zero field emission rate $e(0)$ is determined to be around 10^{-4} s^{-1}, which is in agreement with the experimental results showing that the emission time constant of E1 is almost 1000 s when no bias is applied during the recovery phase. α is a constant, which depends on the applied voltage and on trap potential lowering.

Consistent with the Poole–Frenkel effect [32], the activation energy (E_A) of the detrapping time constant of E1 trap decreases with the square root of the applied gate voltage during recovery, see Fig. 11(a). Also, the dielectric constant was estimated to be 5.7, which is close to the dielectric constant of GaN and AlGaN at high frequency [33].

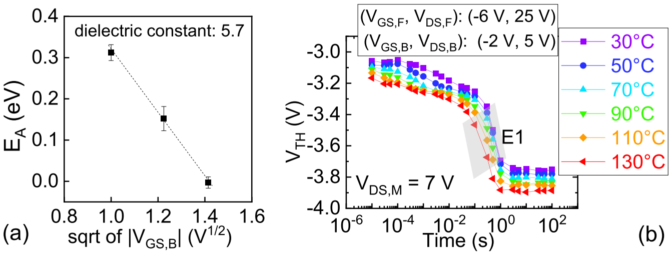

Fig. 11. (a) Activation energy as a function of the square root of the absolute values of the applied gate voltage. (b) V_{TH} transients measured with $V_{G,F} = -6$ V and $V_{D,F} = 25$ V at various temperatures, applying $V_{GS,B} = -2$ V and $V_{DS,B} = 5$ V.

Fig. 11(b) shows the V_{TH} recovery transients after filling at $V_{GS,F} = -6$ V, $V_{DS,F} = 25$ V for 100 s, with a bias of $V_{GSB} = -2$ V, and $V_{DSB} = 5$ V during the recovery phase, as a function of temperature. The detrapping process of E1 practically does not depend on temperature and its E_A is reduced to almost zero.

IV. DISCUSSION AND CONCLUSION

The experimental results reported above can be explained as follows. During quasi-static measurements of the dc output I_D–V_{DS} (V_{GS}) characteristics, starting from pinchoff conditions, V_{DS} is increased from 0 to V_{DSmax}, Consistently, the value of V_{DG} remarkably increases, and electron injection and trapping in deep donor levels in the AlGaN barrier and/or the GaN buffer occurs. The corresponding V_{TH} dynamic transients suggest the presence of two deep levels (E1 and E2) having activation energies of 0.5 and 0.8 eV, respectively (Figs. 6 and 8).

After completing the first curve, the value of V_{GS} is increased, and the V_{DS} staircase starts again from 0 V. For V_{DG} values lower than 4–5 V, the time constant for detrapping is longer than 1 s: since this time is much longer than the measurement time (40 ms), the negative charge under the gate shifts V_{TH} toward positive values, thus inducing a decrease of I_D with respect to the "detrapped" condition, see Fig. 2. However, as V_{GD} is increased beyond approximately 5 V, the emission rate of electrons from donor states in the AlGaN increases exponentially due to the Poole–Frenkel effect, which reduces the activation energy of the traps from 0.5 eV to almost zero, see Figs. 9 and 11 [32]. The detrapping time becomes shorter than the measurement time, V_{TH} becomes more negative, and I_D increases, thus originating a "kink" in the I_D–V_{DS} characteristics. When a reverse scan measurement (from $V_{DS,max}$ to 0 V) is carried out, Fig. 3(a), the high value of V_{DS} makes detrapping time constant very short due to the PF effect so that the "detrapped" state is always measured; then, at low V_{DS}, the electric field is insufficient to cause trapping, so a high value of current is measured along the entire reverse I–V curve.

In other words, the kink is due to a strong dependence of emission time on electric field or voltage (as it occurs for Poole–Frenkel effect [1], as shown in Fig. 12), coupled with a relatively slow sampling and measurement of the parameter analyzer. In fact, when I_D–V_{DS} characteristics are measured

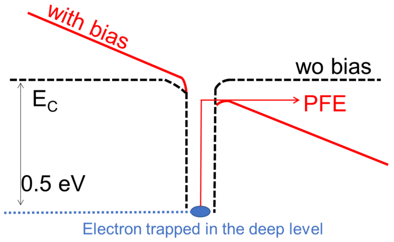

Fig. 12. Schematic electron energy diagram in equilibrium condition when no bias is applied during recovery (black) and in the presence of electric fields, where bias is applied during the recovery phase (red) showing the Poole–Frenkel emission process.

using a fast (1 μs) DP system, kink is not present since detrapping time is longer than 1 μs for any bias condition, see Figs. 4 and 9.

Several authors have attributed the appearance of the kink to Poole–Frenkel effects [1], [34], [35]; however, a detailed analysis of dynamic threshold voltage shift and its dependence on applied bias has not been reported. Our experimental data confirm the model reported in [1]; we attributed the kink to donor traps in the AlGaN, as emission time is more sensitive to V_{GS} than V_{DS}, see Fig. 9; moreover, the activation energy of traps responsible for the kink is around 0.50 eV, a value reported for traps in the AlGaN [36], [37], [38]. Finally, even if we cannot exclude a role for deep acceptors introduced by carbon at nitrogen vacancies (C_N defects), related to hole injection and transport [16] or hole redistribution [39], it should be stressed that the Poole–Frenkel effect on C-doping accelerates hole detrapping [40], leading to faster negative charge build-up due to ionized acceptors, contrarily to what has been observed in the present experiment. We cannot exclude that other mechanisms, not related to Poole–Frenkel effect and involving C traps in the buffer, can be responsible for the kink in other devices, but for the above reasons, we exclude them for the devices under study.

Previous investigations have also suggested that impact ionization [9], [20], [24] may be a possible cause of kink effects; nevertheless, it appears unlikely in the devices studied in this work. This is primarily because impact ionization is a nearly instantaneous process, and such rapid behavior does not align with the very long time constant detected in this work. Even if we assume that long time constants are somehow possible, an increase in temperature should theoretically result in a reduction of the number of hot electrons, consequently slowing down the recovery process. However, the experimental results showed the opposite trend (Fig. 6).

Earlier studies have also reported the presence of kink effects in Fe-doped devices. However, we exclude it, based on the emission time constant of the kink-responsible trap in the devices under study and its strong dependence on gate and drain voltage, both of which are different from the Fe trap. The latter is actually characterized by an emission time constant of ≈10 ms at room temperature with negligible Poole–Frenkel effects [41]. Therefore, Fe-related traps do not play a role in the kink effects observed in the devices studied in this work.

Reported data demonstrate that, although the observation of the kink effect remains an indicator of charge trapping on deep levels or of charge accumulation in a floating, semi-insulating buffer, its occurrence or observation critically depends on measurement conditions; transient measurements are essential for correct understanding of physical phenomena originating the kink, which can be relevant for the operation and reliability of RF AlGaN/GaN HEMTs. Regarding HEMTs with different barrier materials, such as InAl(Ga)N, these can be affected by kink effects as well. In those devices also, if the kink effect is correlated to a voltage-dependent V_{TH} dynamic shift (within the kink bias range), then it is reasonable to assume that barrier traps sensitive to the Poole–Frenkel effect are responsible for the kink.

In summary, new experimental evidence concerning the dynamic behavior of the "kink" phenomenon and its relation to deep levels in AlGaN/GaN HEMTs is presented in this article. This work demonstrates that the kink effect observed in AlGaN/GaN HEMTs is due to a strong dependence of emission time on electric field or voltage (as expected for Poole–Frenkel effect) coupled with a relatively slow sampling and measurement of the parameter analyzer.

REFERENCES

[1] M. Grupen, "Reproducing GaN HEMT kink effect by simulating field-enhanced barrier defect ionization," *IEEE Trans. Electron Devices*, vol. 66, no. 9, pp. 3777–3783, Sep. 2019, doi: 10.1109/TED.2019.2928536.

[2] J.-Y. Choi and J. G. Fossum, "Analysis and control of floating-body bipolar effects in fully depleted submicrometer SOI MOSFETs," *IEEE Trans. Electron Devices*, vol. 38, no. 6, pp. 1384–1391, Jun. 1991, doi: 10.1109/16.81630.

[3] J.-P. Colinge, "Reduction of kink effect in thin-film SOI MOSFETs," *IEEE Electron Device Lett.*, vol. 9, no. 2, pp. 97–99, Feb. 1988, doi: 10.1109/55.2052.

[4] H. J. Park, M. Bawedin, H. G. Choi, and S. Cristoloveanu, "Kink effect in ultrathin FD-SOI MOSFETs," *Solid-State Electron.*, vol. 143, pp. 33–40, May 2018, doi: 10.1016/j.sse.2017.12.002.

[5] C. Canali, C. Tedesco, E. Zanoni, G. Castellaneta, F. Magistrali, and M. Sangalli, "Kink effect, transconductance increase and field enhanced electron emission in AlGaAs/GaAs NEMTs," *Electron. Lett.*, vol. 26, no. 18, p. 1520, 1990, doi: 10.1049/el:19900976.

[6] A. Mazzanti, G. Verzellesi, C. Canali, G. Meneghesso, and E. Zanoni, "Physics-based explanation of kink dynamics in AlGaAs/GaAs HFETs," *IEEE Electron Device Lett.*, vol. 23, no. 7, pp. 383–385, Jul. 2002, doi: 10.1109/LED.2002.1015205.

[7] R. Cuerdo et al., "The kink effect at cryogenic temperatures in deep submicron AlGaN/GaN HEMTs," *IEEE Electron Device Lett.*, vol. 30, no. 3, pp. 209–212, Mar. 2009, doi: 10.1109/LED.2008.2011289.

[8] S. Arulkumaran, T. Egawa, H. Ishikawa, T. Jimbo, and Y. Sano, "Surface passivation effects on AlGaN/GaN high-electron-mobility transistors with SiO_2, Si_3N_4, and silicon oxynitride," *Appl. Phys. Lett.*, vol. 84, no. 4, pp. 613–615, Jan. 2004, doi: 10.1063/1.1642276.

[9] K. Kunihiro, K. Kasahara, Y. Takahashi, and Y. Ohno, "Experimental evaluation of impact ionization coefficients in GaN," *IEEE Electron Device Lett.*, vol. 20, no. 12, pp. 608–610, Dec. 1999, doi: 10.1109/55.806100.

[10] G. Meneghesso, F. Zanon, M. J. Uren, and E. Zanoni, "Anomalous kink effect in GaN high electron mobility transistors," *IEEE Electron Device Lett.*, vol. 30, no. 2, pp. 100–102, Feb. 2009, doi: 10.1109/LED.2008.2010067.

[11] G. Meneghesso, F. Rossi, G. Salviati, M. J. Uren, E. Muñoz, and E. Zanoni, "Correlation between kink and cathodoluminescence spectra in AlGaN/GaN high electron mobility transistors," *Appl. Phys. Lett.*, vol. 96, no. 26, Jun. 2010, Art. no. 263512, doi: 10.1063/1.3459968.

[12] M. Wang and K. J. Chen, "Kink effect in AlGaN/GaN HEMTs induced by drain and gate pumping," *IEEE Electron Device Lett.*, vol. 32, no. 4, pp. 482–484, Apr. 2011, doi: 10.1109/LED.2011.2105460.

[13] M. J. Uren et al., "'Leaky dielectric' model for the suppression of dynamic R_{ON} in carbon-doped AlGaN/GaN HEMTs," *IEEE Trans. Electron Devices*, vol. 64, no. 7, pp. 2826–2834, Jul. 2017, doi: 10.1109/TED.2017.2706090.

[14] M. J. Uren and M. Kuball, "Impact of carbon in the buffer on power switching GaN-on-Si and RF GaN-on-SiC HEMTs," *Jpn. J. Appl. Phys.*, vol. 60, May 2021, Art. no. SB0802, doi: 10.35848/1347-4065/abdb82.

[15] N. Killat, M. J. Uren, D. J. Wallis, T. Martin, and M. Kuball, "Origin of kink effect in AlGaN/GaN high electron mobility transistors: Yellow luminescence and Fe doping," *Appl. Phys. Lett.*, vol. 101, no. 15, pp. 2010–2013, Oct. 2012, doi: 10.1063/1.4757993.

[16] M. Singh, M. J. Uren, T. Martin, S. Karboyan, H. Chandrasekar, and M. Kuball, "'Kink' in AlGaN/GaN-HEMTs: Floating buffer model," *IEEE Trans. Electron Devices*, vol. 65, no. 9, pp. 3746–3753, Sep. 2018, doi: 10.1109/TED.2018.2860902.

[17] M. J. Uren and M. Kuball, "Current collapse and kink effect in GaN RF HEMTs: The key role of the epitaxial buffer," in *Proc. IEEE BiCMOS Compound Semiconductor Integr. Circuits Technol. Symp. (BCICTS)*, Nov. 2020, pp. 1–8, doi: 10.1109/bcicts48439.2020.9392966.

[18] H. Hirshy et al., "Evaluation of pulsed I–V analysis as validation tool of nonlinear RF models of GaN-based HFETs," *IEEE Trans. Electron Devices*, vol. 65, no. 12, pp. 5307–5313, Dec. 2018, doi: 10.1109/TED.2018.2872513.

[19] L. Brunel, N. Malbert, A. Curutchet, N. Labat, and B. Lambert, "Kink effect characterization in AlGaN/GaN HEMTs by DC and drain current transient measurements," in *Proc. Eur. Solid-State Device Res. Conf. (ESSDERC)*, Sep. 2012, pp. 270–273, doi: 10.1109/ESSDERC.2012.6343385.

[20] D. Bisi et al., "Observation of ID-VD kink in N-polar GaN MIS-HEMTs at cryogenic temperatures," *IEEE Electron Device Lett.*, vol. 41, no. 3, pp. 345–348, Mar. 2020, doi: 10.1109/LED.2020.2968875.

[21] J. K. Kaushik, V. R. Balakrishnan, B. S. Panwar, and R. Muralidharan, "On the origin of kink effect in current–voltage characteristics of AlGaN/GaN high electron mobility transistors," *IEEE Trans. Electron Devices*, vol. 60, no. 10, pp. 3351–3357, Oct. 2013, doi: 10.1109/TED.2013.2279158.

[22] R. Vetury, N. Q. Zhang, S. Keller, and U. K. Mishra, "The impact of surface states on the DC and RF characteristics of AlGaN/GaN HFETs," *IEEE Trans. Electron Devices*, vol. 48, no. 3, pp. 560–566, Mar. 2001, doi: 10.1109/16.906451.

[23] S. Arulkumaran, T. Egawa, and H. Ishikawa, "Studies on the influences of I-GaN, N-GaN, P-GaN and InGaN cap layers in AlGaN/GaN high-electron-mobility transistors," *Jpn. J. Appl. Phys.*, vol. 44, no. 5R, p. 2953, May 2005, doi: 10.1143/jjap.44.2953.

[24] X.-H. Ma et al., "Kink effect in current—Voltage characteristics of a GaN-based high electron mobility transistor with an AlGaN back barrier," *Chin. Phys. B*, vol. 23, no. 2, Feb. 2014, Art. no. 027302, doi: 10.1088/1674-1056/23/2/027302.

[25] B. Brar, K. Boutros, R. E. DeWarnes, V. Tilak, R. Shealy, and L. Eastman, "Impact ionization in high performance AlGaN/GaN HEMTs," in *Proc. IEEE Lester Eastman Conf. High Perform. Devices*, Aug. 2002, pp. 487–491, doi: 10.1109/lechpd.2002.1146791.

[26] S. C. Binari et al., "Trapping effects and microwave power performance in AlGaN/GaN HEMTs," *IEEE Trans. Electron Devices*, vol. 48, no. 3, pp. 465–471, Mar. 2001, doi: 10.1109/16.906437.

[27] P. Altuntas et al., "On the correlation between kink effect and effective mobility in InAlN/GaN HEMTs," in *Proc. 9th Eur. Microw. Integr. Circuit Conf.*, Oct. 2014, pp. 88–91, doi: 10.1109/EuMIC.2014.6997798.

[28] S. D. Nsele, L. Escotte, J.-G. Tartarin, S. Piotrowicz, and S. L. Delage, "Broadband frequency dispersion small-signal modeling of the output conductance and transconductance in AlInN/GaN HEMTs," *IEEE Trans. Electron Devices*, vol. 60, no. 4, pp. 1372–1378, Apr. 2013, doi: 10.1109/TED.2013.2248158.

[29] E. Zanoni et al., "Failure physics and reliability of GaN-based HEMTs for microwave and millimeter-wave applications: A review of consolidated data and recent results," *Phys. Status Solidi A*, vol. 219, no. 24, Dec. 2022, Art. no. 2100722, doi: 10.1002/pssa.202100722.

[30] M. H. Wong and U. K. Mishra, *N-Polar III-Nitride Transistors*, vol. 102, 1st ed. Amsterdam, The Netherlands: Elsevier, 2019.

[31] D. Bisi et al., "High-voltage double-pulsed measurement system for GaN-based power HEMTs," in *Proc. IEEE Int. Rel. Phys. Symp.*, Jun. 2014, pp. CD.11.1–CD.11.4, doi: 10.1109/IRPS.2014.6861130.

[32] O. Mitrofanov and M. Manfra, "Poole-Frenkel electron emission from the traps in AlGaN/GaN transistors," *J. Appl. Phys.*, vol. 95, no. 11, pp. 6414–6419, Jun. 2004, doi: 10.1063/1.1719264.

[33] D. D. Manchon Jr., A. S. Barker Jr., P. J. Dean, and R. B. Zetterstrom, "Optical studies of the phonons and electrons in gallium nitride," *Solid State Commun.*, vol. 8, no. 15, pp. 1227–1231, 1970, doi: 10.1016/0038-1098(70)90365-0.

[34] C.-h. Chen et al., "The interplay of thermal, time and Poole–Frenkel emission on the trap-based physical modeling of GaN HEMT drain characteristics," in *Proc. IEEE Compound Semiconductor Integr. Circuit Symp. (CSICS)*, Oct. 2017, pp. 1–4, doi: 10.1109/CSICS.2017.8240427.

[35] J. Mukherjee, A. Malik, S. Vinayak, D. S. Rawal, and R. S. Dhaka, "Deep trap characterization and the kink effect in AlGaN/GaN HEMTs," *IETE Tech. Rev.*, vol. 39, no. 2, pp. 335–342, Mar. 2022, doi: 10.1080/02564602.2020.1853619.

[36] M. Gassoumi, B. Grimbert, C. Gaquiere, and H. Maaref, "Evidence of surface states for AlGaN/GaN/SiC HEMTs passivated Si_3N_4 by CDLTS," *Semiconductors*, vol. 46, no. 3, pp. 382–385, Mar. 2012, doi: 10.1134/s1063782612030104.

[37] D. Kindl et al., "Deep defects in GaN/AlGaN/SiC heterostructures," *J. Appl. Phys.*, vol. 105, no. 9, May 2009, Art. no. 093706, doi: 10.1063/1.3122290.

[38] W. I. Lee, T. C. Huang, J. D. Guo, and M. S. Feng, "Effects of column III alkyl sources on deep levels in GaN grown by organometallic vapor phase epitaxy," *Appl. Phys. Lett.*, vol. 67, no. 12, pp. 1721–1723, Sep. 1995, doi: 10.1063/1.115028.

[39] N. Zagni et al., "'Hole Redistribution' model explaining the thermally activated R_{ON} stress/recovery transients in carbon-doped AlGaN/GaN power MIS-HEMTs," *IEEE Trans. Electron Devices*, vol. 68, no. 2, pp. 697–703, Feb. 2021, doi: 10.1109/TED.2020.3045683.

[40] N. Zagni, M. Cioni, F. Iucolano, M. Moschetti, G. Verzellesi, and A. Chini, "Experimental and numerical investigation of Poole–Frenkel effect on dynamic R_{ON} transients in C-doped p-GaN HEMTs," *Semicond. Sci. Technol.*, vol. 37, no. 2, Feb. 2022, Art. no. 025006, doi: 10.1088/1361-6641/ac4113.

[41] M. Cioni et al., "Electric field and self-heating effects on the emission time of iron traps in GaN HEMTs," *IEEE Trans. Electron Devices*, vol. 68, no. 7, pp. 3325–3332, Jul. 2021, doi: 10.1109/TED.2021.3081613.

Open Access funding provided by 'Università degli Studi di Padova' within the CRUI CARE Agreement